A Stochastic Finite Element Approach on Creep of Rock Salt

M. Grehn, A. Fau, U. Nackenhorst
mathias.grehn@ibnm.uni-hannover.de

Abstract

A robust computational material model for rock salt with a stochastic approach for Young's modulus is developed to predict rock salt behavior during a creep test. The uncertain input data as well as the unknown displacement fields are described by Hermite polynomial chaos. The numerical problem is solved using Stochastic Finite Element Procedure. The material model is able to reproduce the experimental results during the two first creep periodes including the scattering of experimental creep curves.

Keywords: Stochastic Finite Element Method, Polynomial Chaos, Creep Test, Viscoelastic, Rock Salt

1 Introduction

Old salt domes are used as reservoirs for toxic and nuclear waste in Germany. Nuclear waste has a long half-life time, so the mechanical stability of salt domes has to be guaranteed for a long period. In the last decades, a large expertise in the mechanical behavior of rock salt was gained. This led to a variety of material models, which may be based on a macroscopic phenomenological approach [1], derived from Burger's modified model [2], or from micromechanics using the composite dilatancy model [3, 4, 5, 6] for examples.
However, from experimental results obtained during creep tests for rock salt from Asse mine in Germany [7] reproduced in Figure 1 it can be seen that the material properties are subject to large variation as also observed by [4, 8]. The goal of this paper is to reproduce this creep test including the scattering of experimental data by introducing a stochastic material model for rock salt.

2 Origin of uncertainties

To analyze numerically the behaviour of rock salt, we refer to a material model based on different established works from the literature [7, 9, 5, 6].

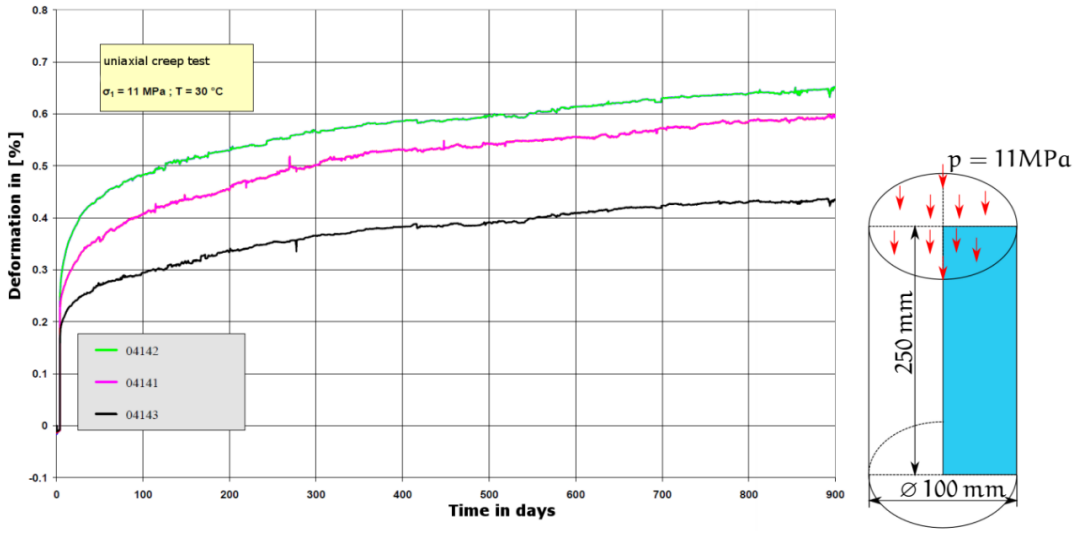

a) Creep curve b) Experimental setup

Figure 1: Experimental uniaxial creep test for three samples of Asse rock salt reproduced after [7]

2.1 Material model

The analysis of the creep test can be split into three parts as illustrated in Figure 2 [10]. During the primary creep period (I), the dislocations move in the lattice structure of the crystal salt. The strain rate is relatively high, but it slows down by increasing time. In the secondary or steady-state creep period (II) the dislocation density increases leading to an increasing resistance. The strain rate is nearly constant. The tertiary creep period (III) is characterized by an exponentially increasing of the strain rate. We focus here only on the two first creep periods to reproduce the experimental results previously presented.

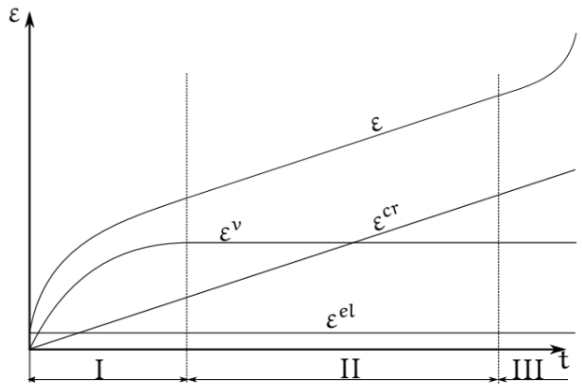

Figure 2: Analysis of the creep behavior of rock salt

The material model is based on an additive split of the strain tensor $\boldsymbol{\varepsilon}$:

$$\boldsymbol{\varepsilon} = \boldsymbol{\varepsilon}^{el} + \boldsymbol{\varepsilon}^{v} + \boldsymbol{\varepsilon}^{cr}. \tag{1}$$

The elastic strain tensor $\boldsymbol{\varepsilon}^{el}$ and the viscous strain tensor $\boldsymbol{\varepsilon}^{v}$ describe the primary creep period. The steady-state creep period is described by the creep strain tensor $\boldsymbol{\varepsilon}^{cr}$. We can reproduce the viscoelastic part for one-dimensional systems by springs of stiffnesses E_i and dampers of coefficients η_i using a generalized Maxwell model and the following free energy function [9]:

$$\psi(\boldsymbol{\varepsilon}, \boldsymbol{q}_i) = W^{\circ}(\boldsymbol{\varepsilon}) + \sum_{i=1}^{N_{MW}} \boldsymbol{q}_i \cdot \tilde{\boldsymbol{\varepsilon}} + \Xi \left(\sum_{i=1}^{N_{MW}} \boldsymbol{q}_i \right). \tag{2}$$

The function W° is the initial stored energy function. The internal variables $\boldsymbol{q}_i$ characterize the viscoelastic response and $\tilde{\boldsymbol{\varepsilon}} = \boldsymbol{\varepsilon} - \frac{1}{3} tr(\boldsymbol{\varepsilon})$ is the deviatoric strain. N_{MW} is the number of Maxwell elements. We consider one spring of stiffness E_{∞} connected in parallel with two Maxwell elements whose stiffnesses are respectively E_1 and E_2. The total Young modulus E is computed as a summation of all single Young's modulus:

$$E = E_{\infty} + \sum_{i=0}^{2} E_i. \tag{3}$$

The creep behavior of rock salt for the deviatoric part of the creep strain tensor is described by Norton's law:

$$\dot{\tilde{\varepsilon}}^{cr} = A \exp\left(\frac{-Q}{RT}\right) \cdot \left(\sigma^{vM}\right)^{N}, \tag{4}$$

where N is a material parameter and σ^{vM} denotes the von Mises stress. The temperature dependency of the creep curve is described by Arrhenius equation, which is linked multiplicative with the creep rates. The pre-exponential factor A is determined by experiments. R denotes the universal gas constant and T the absolute temperature. The macroscopic activation energy Q is provided by [5].

Experiments [7, 6] show that for rock salt, the volumetric deformation depends on the state of stress in comparison with the dilatancy boundary. This material behavior is described by the functional r_v introduced in [7]:

$$r_v = \begin{cases} 3\left[\frac{\tau_{okt} - \tau_D}{\sigma_{okt}}\right]^2 & \text{for } \tau_{okt} > \tau_D \\ 0 \quad \text{otherwise.} \end{cases} \tag{5}$$

The function τ_D represents the dilatancy boundary equation [7]. τ_{okt} is the octahedral shear stress and σ_{okt} is the octahedral normal stress. When the state of stress is below the dilatancy boundary, the deformation is at constant volume, otherwise arises the volumetric part of the creep strain tensor defined as:

$$\dot{\varepsilon}^{cr,vol} = r_v \, \dot{\tilde{\varepsilon}}^{cr}. \tag{6}$$

In loosened rock salt the moisture has a big influence on the creep rate. This behavior is modeled by the following equations [7]:

$$
\begin{aligned}
f_\Phi &= c_{\Phi 1} \sinh\left(c_{\Phi 2}\, \Phi\right), \\
f_c &= \begin{cases} \left[1 + \left(\frac{\sigma_3}{\sigma_u}\right)^{c_{fc1}\, \tau_{okt}}\right]^{-\left(\frac{c_{fc2}}{1+\left(\frac{\tau_{okt}}{\sigma_u}\right)}\right)^2} & \text{for } \sigma_3 \geq 0 \\ 1 \quad \text{otherwise,} \end{cases} \\
F_h &= 1 + f_\Phi\, f_c.
\end{aligned}
\tag{7}
$$

The factor F_h, which is linked multiplicative with the creep rates, sets together two effects. The first part f_Φ describes the influence of relative humidity Φ on the creep rate. The second one f_c takes into account the influence of minimum principal stress σ_3 and the octahedral shear stress τ_{okt}. The other components in this equation are material parameters defined by [6].

To predict the primary and the secondary creep behavior of rock salt over long time the evolution equations must be solved efficiently by numerical techniques. We apply finite element technique to an axisymmetric geometrical model to reduce the computational efforts. We use for the primary creep periode the algorithm introduced in [9] and for the secondary creep periode the one proposed in [11].

2.2 Identifying the random parameters

The three uniaxial creep tests performed by [7] have the same set up with an axial stress equal to 11 MPa, see Figure 1. We investigate which material parameters have to be considered different for the three rock salt samples to reproduce consistently the scattering of the experimental curves.
Based on Equation 4 we can see that a scattering of the material parameters A or N or of the relative humidity Φ changes the slope of the secondary creep period, which is contradictory with the experimental results. The stiffness of the first spring E_∞ in the generalized Maxwell model characterizes the asymptotic solution $\varepsilon^v(t = \infty)$ for the second creep period. For this reason the free energy function in Equation 2 will be stochastically distributed assuming an uncertain Young's modulus E_∞. The stochastic approaches chosen to describe E_∞ as a random field and to solve the stochastic finite element problem are introduced in the following section.

3 Stochastic Finite Element Approach

For solving the boundary value problem, we use the stochastic finite element method [12] with the aid of polynomial chaos expansions to describe the input random field $E_\infty(\theta)$ as well as the displacement random field $u(\theta)$. Each random quantity is characterized by θ.

3.1 Representation of the random input

The Young modulus $E_\infty(\theta)$ is approximated as a Hermite polynomial chaos (PC) series expansion:

$$E_\infty(\theta) \approx \sum_{i=0}^{p} a_i H_i\left(\xi(\theta)\right), \tag{8}$$

where p is the order of Hermite polynomials H_i defined as in [13]:

$$H_i\left(x\right) = (-1)^i \frac{1}{\varphi\left(E_\infty\right)} \frac{d^i \varphi\left(x\right)}{dx^i}, \tag{9}$$

$\varphi\left(x\right) = \frac{1}{\sqrt{2\pi}} e^{-\frac{x^2}{2}}$ is the standard normal probability density function (PDF). To compute the coefficients a_i in Equation 8, we use the projection method [13]. The Hermite polynomials are orthogonal with respect to the Gaussian measure. For a probability space with dimension M equals to 1 one obtains

$$\mathbb{E}[E_\infty H_i\left(\xi(\theta)\right)] = a_i\, \mathbb{E}[H_i^2\left(\xi(\theta)\right)], \tag{10}$$

where $\mathbb{E}$ is the mean operator and $\mathbb{E}[H_i^2\left(\xi(\theta)\right)] = i!$. With help of the transformation to the standard normal space $E_\infty \to \xi : F_x(E_\infty) = \Phi(\xi(\theta))$, we can write the random variable as following:

$$E_\infty\left(\xi(\theta)\right) = F_x^{-1}(\Phi(\xi(\theta))). \tag{11}$$

The coefficients $\{a_i, i = 0, ..., \infty\}$ are computed as:

$$a_i = \frac{1}{i!}\mathbb{E}[[E_\infty\left(\xi(\theta)\right) H_i\left(\xi(\theta)\right)] = \frac{1}{i!}\int_{\mathbb{R}} F_x^{-1}(\Phi(t)) H_i(t)\varphi(t)dt. \tag{12}$$

Therefore, for the specific cases of normal or log-normal distributions, we get:

$$\begin{aligned} &\text{if } E_\infty(\theta) \equiv N\left(\mu_{E_\infty}, \sigma_{E_\infty}\right), \qquad a_0 = \mu_{E_\infty},\, a_1 = \sigma_{E_\infty},\, a_i = 0 \quad for \quad i \geq 0 \\ &\text{if } E_\infty(\theta) \equiv LN\left(\lambda_{E_\infty}, \zeta_{E_\infty}\right), \qquad a_i = \frac{\zeta_{E_\infty}^i}{i!} \exp\left[\lambda_{E_\infty} + \frac{1}{2}\zeta_{E_\infty}^2\right] \quad for \quad i \geq 0, \end{aligned} \tag{13}$$

where the index i goes from 0 to P the dimension of PC basis. The parameters $\lambda_{E_\infty}, \zeta_{E_\infty}$ for log-normal distributions depend on the mean and the standard deviation see [13]. The size P of the polynomial chaos basis is given by:

$$P = \frac{(M+p)!}{M!p!}. \tag{14}$$

Based on the independence of the random variable $\xi(\theta)$ inside the PC expansion, we can compute the multi-dimensional basis:

$$\psi_\alpha = \prod_{i=1}^{M} H_{\alpha_i}, \tag{15}$$

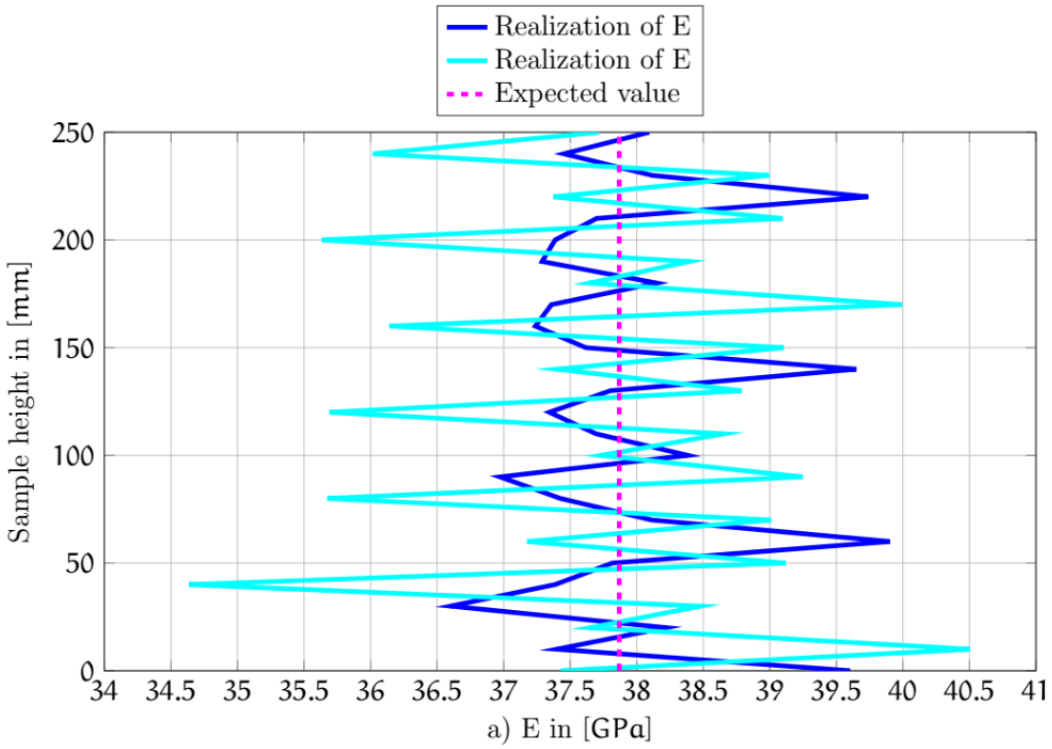

Figure 3: Two realizations of Young's modulus $[GPa]$ field for a rock salt sample.

with $\alpha_i \geq 0$ and $\sum_{i=1}^{M} \alpha_i \leq p$ as a product of one-dimensional basis. An illustrative transmission of an urn problem is introduced in [13]. Thus the PC can be written as:

$$E_\infty = \sum_{i=0}^{P-1} \hat{E}_{\infty_i} \psi_i \left(\xi(\theta)\right), \tag{16}$$

where $\hat{E}_\infty$ is the deterministic PC-coefficient.
The considered creep test results are not statistically representative to have a trustable representation of material uncertainties, a large number of experimental data would be required. We assume for E_∞ a normal (N) or a lognormal (LN) distribution. The mean of the Young modulus μ_{E_∞} is estimated as the parameter reproducing the mean of the three experimental results, i.e. $\mu_{E_\infty} = 2,140$ GPa. The standard deviation σ_{E_∞} is computed such that at least about 60 % of the probabilistic creep test results are between the two extreme experimental curves i.e. $\sigma_{E_\infty} = 0,535$ GPa.
In Figure 3 two realizations of the Young modulus random field ($\mu_E = 37,8$ GPa and $\sigma_E = 0,535$ GPa) are shown over the cross section $x = 30\,mm$ for a polynomial chaos basis up to order 2. For all the Gauss points, Young's modulus values are scattered around the mean value, which is represented by a dashed line.

3.2 Estimation of the random displacement field

The linearization of the deterministic discrete FEM for static problems yields a linear system of size $N_d \times N_d$ where N_d is the number of degrees of freedom in the

FEM geometry:

$$\boldsymbol{K}\Delta\boldsymbol{u} = \boldsymbol{r} - \boldsymbol{r}^{int}, \tag{17}$$

$\boldsymbol{K}$ is the total stiffness matrix, $\boldsymbol{u}$ is the displacement field, $\boldsymbol{r}$ and $\boldsymbol{r}^{int}$ are respectively the vectors of external and internal forces.
In the stochastic finite element model we assume the loading and the geometry as certain. We introduce input random variables for material properties as a PC expansion:

$$\boldsymbol{K}(\theta)\Delta u(\theta) = \boldsymbol{r} - \boldsymbol{r}^{int}(\theta), \tag{18}$$

where $\boldsymbol{K}(\theta)$ is the stochastic stiffness matrix. Details to compute the total stiffness matrix can be found in [12, 13, 14]. By expanding each component of the unknown displacement field as:

$$u(\theta) \approx \sum_{i=0}^{P-1} u_i \psi_i \left(\xi(\theta)\right), \tag{19}$$

we get the following discretized problem:

$$\sum_{i=0}^{P-1} \hat{\boldsymbol{K}}_i \psi_i \left(\xi\right) \sum_{j=0}^{P-1} \Delta\hat{\boldsymbol{u}}_j \psi_j \left(\xi\right) = \sum_{j=0}^{P-1} \hat{\boldsymbol{r}}_j \psi_j \left(\xi\right) - \sum_{j=0}^{P-1} \hat{\boldsymbol{r}}_j^{int} \psi_j \left(\xi\right) \tag{20}$$

where $\hat{\cdot}$ represents the nodal discretization. The resulting linear system:

$$\begin{bmatrix} \boldsymbol{K}_{0,0} & \cdots & \boldsymbol{K}_{0,P-1} \\ \vdots & \ddots & \vdots \\ \boldsymbol{K}_{0-1,0} & \cdots & \boldsymbol{K}_{P-1,P-1} \end{bmatrix} \cdot \begin{bmatrix} \Delta\boldsymbol{u}_0 \\ \vdots \\ \Delta\boldsymbol{u}_{P-1} \end{bmatrix} = \begin{bmatrix} \boldsymbol{r}_1 \\ \vdots \\ \boldsymbol{r}_{P-1} \end{bmatrix} - \begin{bmatrix} \boldsymbol{r}_1^{int} \\ \vdots \\ \boldsymbol{r}_{P-1}^{int} \end{bmatrix} \tag{21}$$

has a size $(N_d * P) \times (N_d * P)$. The mean value contribution is contained in the main diagonal elements [13]. Considering a probability space of dimension 1, the size of the linear system is $(N_d * \frac{(p+1)!}{p!}) \times (N_d * \frac{(p+1)!}{p!})$. The size of the linear system is largely increased considering random input data. For a case using 156 nodes, the size of the deterministic stiffness matrix is 312×312, whereas for a polynomial chaos of order 1, the size of the stochastic stiffness matrix is 624×624. But, these matrices are symmetric and sparse matrices.
To solve the large system of equation, we can choose to use a direct solver or an iterative scheme as for example the Gauss-Seidel PC solver introduced in [15, 16]. The advantage of the direct solver is that the equation system must be solved only one time but it may face memory problems for very large stiffness matrix. Here, as we tackle an axisymmetric case with a unique random field, we can use a direct solver for this calculation.

4 Numerical results for the creep test

We reproduce the creep test using the parameters listed in Table 8:

Parameter	Value	Unit
μ_E	2.140	GPa
σ_E	0.535	GPa
P	3	-
Distribution	log-normal	-
Realizations	300	-

Table 8: Stochastic parameters

The results of the stochastic finite element calculation of the creep test are illustrated in Figure 4. The robust stochastic numerical model for rock salt allows to reproduce the test for a time period of 900 days. The dashed line represents the mean of the deformation of the rock salt sample. With the assumed distribution (see Section 3.1), $64,2\,\%$ of the stochastic deformation lies between the two extreme experimental curves reproduced by the black lines.

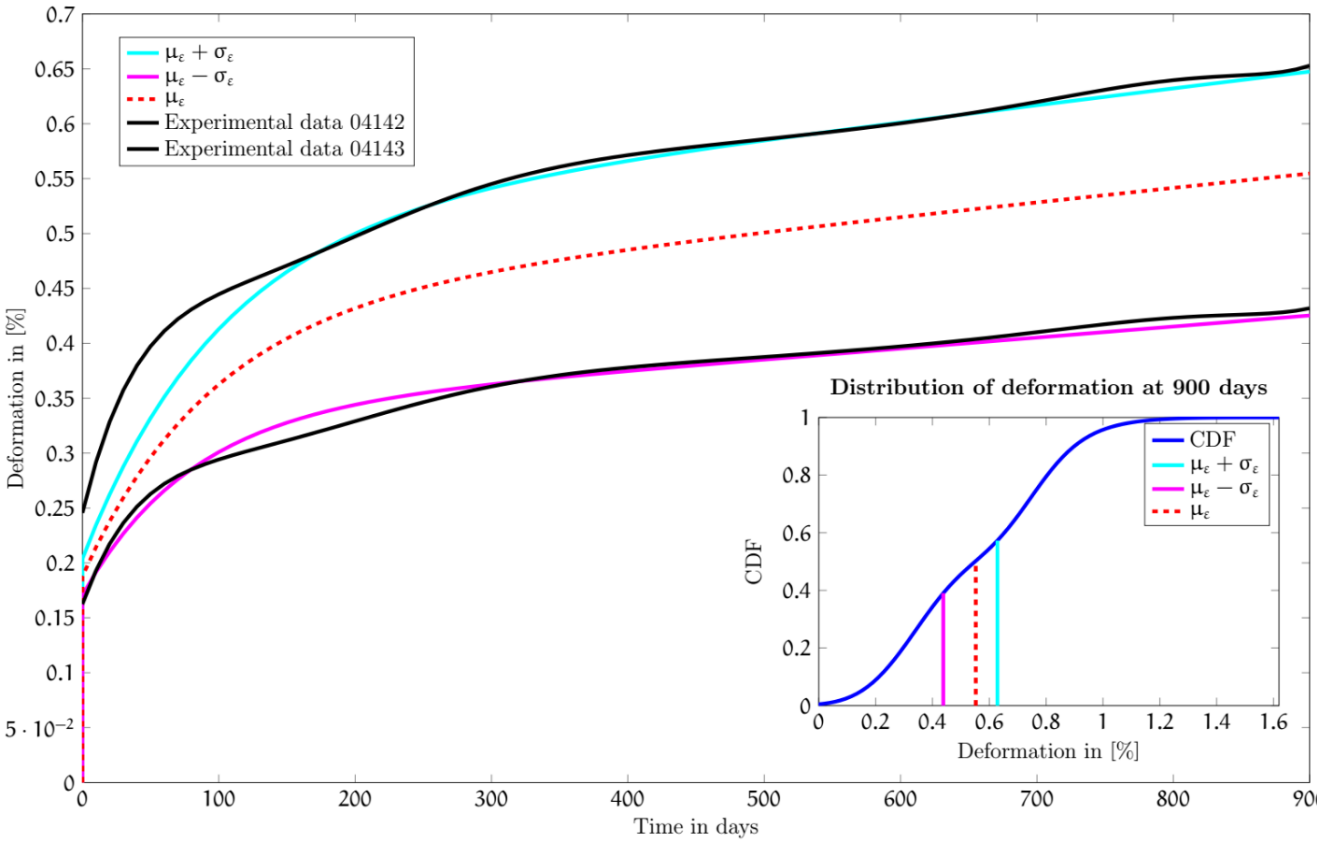

Figure 4: Distribution of strain field

4.1 Convergence of the expected value

We investigate the convergence of our computations with respect to the number of realizations. The calculation parameters are summarized in Table 9:

Parameter	Value	Unit
μ_{E_∞}	2.140	GPa
σ_{E_∞}	0.535	GPa
r	2	-
Realizations	[3,...,2187]	-

Table 9: Stochastic parameters

Figures 5a and 5b show the means of Young's modulus E_∞ in $[GPa]$ and of the deformation in [%] at 900 days. The convergence behavior for the input and output random fields are quite similar. We consider they reach an acceptable error for 200 realizations. By increasing the number of realizations, the computational time becomes larger. From three to 2000 realizations, the computational times has been multiplied by nine. For further computations we consider a number of 300 realizations as a good compromise between accuracy and computing time. As we

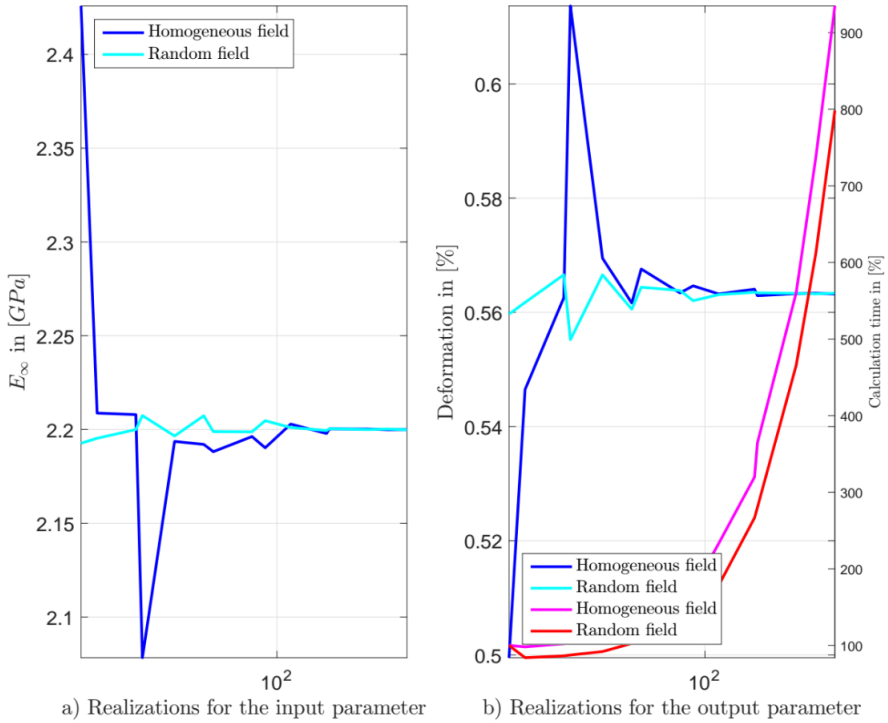

a) Realizations for the input parameter b) Realizations for the output parameter

Figure 5: Convergence of the expected value for the input parameter and the deformation.

assume here an axisymmetric geometry, we impose a priori a specific structure for the random field. So, we also investigate the results considering the Young modulus

as a random variable and a homogeneous field. We see that this assumption does not influence the results largely. Homogeneous field using a unique random variable convergences by around 500 realizations whereas the computations for random field converge by around 200 realizations to the expected value. For this simple creep test, a homogeneous field allows to describe correctly the behavior. The development of the random field has been done as a preparation to compute damage for the third creep period.

5 Conclusions

In this paper, we have presented a numerically robust stochastic material model to predict the creep behavior for rock salt. We can reproduce the creep tests shown in [7] and [6].
Here, we have considered homogeneous random fields. We could extend our computations to heterogeneous random fields to include for example some localized impurities. Further work is to simulate the third creep period of the experimental tests and to predict the damage in real salt domes within a stochastic framework.

References

[1] Z. Hou, R. Wolters, and U. Düsterloh. Die Modellierung des mechanischen Verhaltens von Steinsalz: Vergleich aktueller Stoffgesetze und Vorgehensweisen. BMBF-Verbundvorhaben, Ergebnisbericht zu Teilvorhaben 1, Förderkennzeichen 02 C 1004, 2007.

[2] R. Günther, W. Minkley, and K. Salzer. Die Modellierung des mechanischen Verhaltens von Steinsalz: Vergleich aktueller Stoffgesetze und Vorgehensweisen. BMBF-Verbundvorhaben, Ergebnisbericht zu Teilvorhaben 1, Förderkennzeichen 02 C 1004, 2007.

[3] A. Hampel, U. Hunsche, P. Weidinger, and W. Blum. Description of the Creep of Rock Salt with the Composite Model - II. Steady-State Creep. Series on soil and rock mechanics, 1996.

[4] U. Hunsche. Visco-Plastic Behaviour of Geomaterials, chapter Uniaxial and Triaxial Creep and Failure Tests on Rock: Experimental Technique and Interpretation, pages 1-53. Springer Vienna, Vienna, 1994.

[5] P. Weidinger, A. Hampel, W. Blum, and U. Hunsche. Creep behaviour of natural rock salt and its description with the composite model. Materials Science and Engineering: A, 234236:646 - 648, 1997.

[6] A. Hampel. Die Modellierung des mechanischen Verhaltens von Steinsalz: Vergleich aktueller Stoffgesetze und Vorgehensweisen. BMBF-Verbundvorhaben, Ergebnisbericht zu Teilvorhaben 1, Förderkennzeichen 02 C 1004, 2006.

[7] U. Heemann and O. Schulze. Die Modellierung des mechanischen Verhaltens von Steinsalz: Vergleich aktueller Stoffgesetze und Vorgehensweisen. BMBFVerbundvorhaben, Ergebnisbericht zu Teilvorhaben 1, Förderkennzeichen 02 C 1004, 2007.

[8] G. Wang, L. Zhang, Y. Zhang, and G. Ding. Experimental investigations of the creepdamagerupture behaviour of rock salt. International Journal of Rock Mechanics and Mining Sciences, 66:181 - 187, 2014.

[9] J. C. Simo and T. J. R. Hughes. Computational Inelasticity. Springer, Berlin,1998.

[10] M.L. Jeremic. Rock Mechanics in Salt Mining. Taylor and Francis, 1994.

[11] H. L. Schreyer. On time integration of viscoplastic constitutive models suitable for creep. Int. J. Numer. Meth. Engng., 2001.

[12] O.C. Zienkiewicz and R.L. Taylor. Finite Element Method (5th Edition) Volume 1 - The Basis. Elsevier, 2000.

[13] B. Sudret, M. Berveiller, and M. Lemaire. A stochastic finite element procedure for moment and reliability analysis. European Journal of Computational Mechanics, 2012.

[14] B. Sudret and A. Kiureghian. Stochastic Finite Element Methods and Reliability A State-of-the-Art Report. Department of civil and environmental engineering university of california, 2000.

[15] Y. Saad. Iterative Methods for Sparse Linear Systems: Second Edition. EngineeringPro collection. Society for Industrial and Applied Mathematics (SIAM, 3600 Market Street, Floor 6, Philadelphia, PA 19104), 2003.

[16] D.M. Young and W. Rheinboldt. Iterative Solution of Large Linear Systems. Computer science and applied mathematics. Elsevier Science, 2014.

M. Grehn, Leibniz Universität Hannover, Institute of Mechanics and Computational Mechanics, Appelstr. 9a, 30167 Hannover

A. Fau, Leibniz Universität Hannover, Institute of Mechanics and Computational Mechanics, Appelstr. 9a, 30167 Hannover

U. Nackenhorst, Leibniz Universität Hannover, Institute of Mechanics and Computational Mechanics, Appelstr. 9a, 30167 Hannover